Journal of Alloys and Compounds 889 (2021) 161819

Contents lists available at ScienceDirect

Journal of Alloys and Compounds

journal homepage: www.elsevier.com/locate/jalcom

Comparative study of structural and magnetic properties of ribbon and bulk $Ni_{55}Fe_{19}Ga_{26}$ Heusler alloy

A.F. Manchón-Gordón[a], J.J. Ipus[a], M. Kowalczyk[b], J.S. Blázquez[a,*], C.F. Conde[a], P. Švec[c], T. Kulik[b], A. Conde[a]

[a] Dpto. Física de la Materia Condensada, ICMSE-CSIC, Universidad de Sevilla, P.O. Box 1065, 41080 Sevilla, Spain
[b] Faculty of Materials Science and Engineering, Warsaw University of Technology, 141 Wołoska st., 02-507 Warsaw, Poland
[c] Institute of Physics, Slovak Academy of Sciences, Dúbravská cesta 9, 845 11 Bratislava 45, Slovak Republic

ARTICLE INFO

Article history:
Received 15 June 2021
Received in revised form 5 August 2021
Accepted 30 August 2021
Available online 1 September 2021

Keywords:
Magnetic shape memory alloys
Martensite structure
Magnetostructural transition
Heusler alloy
Melt-spinning

ABSTRACT

The influence of the fabrication method on the magnetostructural properties of a $Ni_{55}Fe_{19}Ga_{26}$ Heusler alloy, obtained both as a ribbon, by melt-spinning, and as a pellet, by arc-melting, has been analyzed. It has been found that, while the arc-melting technique leads to the precipitation of the gamma phase and to a non-modulated martensite structure, the alloy prepared by melt-spinning presents a fully 14M modulated martensitic structure at room temperature. The tetragonal non-modulated martensite in the arc-melted bulk sample transforms into the 14M structure after a long thermal treatment (at 1073 K for 24 h) and subsequent quenching. Characteristic temperatures of the martensitic transformation are higher for melt-spun ribbons than for bulk sample, due to the precipitation of the gamma phase and consequent different martensite composition. However, while the martensitic transformation temperature is practically constant in the case of the bulk sample, it changes by ~ 150 K in the case of the ribbon sample submitted to the same thermal treatment applied to bulk samples. Finally, it was found that the martensitic transformation occurs in the paramagnetic regime of both types of samples.

1. Introduction

Since the pioneer work of Ullakko et al. [1], interest in research and development of Ni-Mn-Ga magnetic shape memory alloys is increasing [2–5]. However, the Ni-Fe-Ga system has also attracted great attention due to its better ductility, attributed to the precipitation of the secondary γ phase [6], which could inhibit the twin boundary motion and limit the shape memory properties of the system. These alloys show remarkable properties, such as recently reported elastocaloric effects [7–9].

Studies on Ni-Fe-Ga alloys have so far mostly focused on bulk polycrystalline materials produced by arc-melting and submitted to high temperature heat treatments for compositional homogenization [10–14]. However, this process results in various problems, such as decomposition or precipitation of other unexpected phases, which negatively affect the functional properties of the alloy. Rapid quenching preparation techniques, like melt-spinning, are an effective single step process to produce textured polycrystalline ribbons without the precipitation of the secondary γ phase [15,16]. Moreover, it makes possible to shorten (or even to avoid) long annealing treatments, which lead to a reduction of the fabrication time and cost.

To our knowledge, little data exist concerning the effect of the fabrication process on structure, magnetostructural behavior and temperatures of martensitic transformation, MT, in Ni-Fe-Ga based alloys, although this kind of studies can be found in Ni-Mn-Sn based Heusler compounds [17,18]. It is also possible to find comparatives studies of bulk and powder samples in Ni-Fe-Ga alloys [19]. Moreover, it has been studied the effect of the quenching rate on the magnetic and martensite properties of Ni-Fe-Ga melt-spun ribbons [16,20] and, recently, the effect of the existence of vacancies in polycrystalline Ni-Fe-Ga systems [21]. Particularly, in $Ni_{55}Fe_{19}Ga_{26}$ composition, MT is observed slightly above room temperature [22]. The present study is devoted to analyze the influence of the fabrication process on structure and magnetostructural behavior and on the temperature of MT in a $Ni_{55}Fe_{19}Ga_{26}$ Heusler alloy obtained both in ribbon shape by melt-spinning and as-pellet by arc-melting.

* Corresponding author.
E-mail address: jsebas@us.es (J.S. Blázquez).

https://doi.org/10.1016/j.jallcom.2021.161819
0925-8388/

2. Experimental

The alloy with nominal composition $Ni_{55}Fe_{19}Ga_{26}$ was prepared in an induction furnace using high-purity elements (> 99.9%). The ingots were melted several times in order to ensure homogeneity. Then, about 30 g of the ingot was induction melted in a quartz tube under Ar atmosphere and ejected onto a rotating wheel with a surface velocity of ~25 m/s. The thickness and width of the ribbon are about 30 µm and 3 mm, respectively. Microstructural characterization and stability of $Ni_{55}Fe_{19}Ga_{26}$ melt spun Heusler alloy can be found elsewhere [23]. A polycrystalline $Ni_{55}Fe_{19}Ga_{26}$ alloy was also prepared from 5 g of a mixture of high-purity constituent elements (> 99.9%) that were melted four times under Ar atmosphere in an arc furnace. Parts of the ingot were cut and annealed at 1073 K for 24 h in a quartz ampoule filled with Ar and then immediately quenched in water. This sample will be called TTB (Thermally Treated Bulk). For comparison, the same thermal treatment was performed to the ribbon, TTR (Thermally Treated Ribbon).

The chemical composition of the samples was analyzed by X-ray fluorescence (XRF) using an EAGLE III instrument with an anticathode of Rh. The martensitic transformation start temperature, M_{start}, as well as the austenite transformation start temperature, A_{start}, were determined by differential scanning calorimetry (DSC) using a Perking-Elmer DSC 7 under Ar flow and equipped with a cooling system (heating/cooling rate of ± 20 K/min). The heating rate was chosen in order to optimize the signal-noise ratio of the DSC measurements. Measured temperatures were corrected using the melting temperatures of an In standard (429.75 K).

The microstructural characterization was carried out by X-ray diffraction (XRD) and scanning electron microscopy (SEM). XRD measurements were performed in a Bruker D8 I diffractometer (Cu-Kα, λ = 1.5406 Å). SEM observations were developed in a FEI Teneo microscope operating at 20 kV.

Magnetization measurements were performed in a vibrating sample magnetometer (standard option of a Quantum Design Physical Properties Measurement System, PPMS) applying different magnetic fields and a heating/cooling rate of ± 1 K/min.

3. Results

3.1. Ribbon sample

The studied $Ni_{55}F_{19}Ga_{26}$ Heusler as-spun ribbon produced by melt spinning shows a typical columnar structure in the fracture cross section (Fig. 1). This consists of grains crystallizing in contact with the wheel, followed by an ordered columnar microstructure perpendicular to the ribbon surface. This is a sign of the quick crystallization and fast growth kinetics of the sample. Perpendicularly to the ribbon surface, the size of the observed grains is as large as the ribbon thickness and their size in the ribbon plane is about 2 µm.

Chemical composition of the ribbon has been evaluated by XRF technique, while electron valence concentration per atom, e/a, was calculated from the sum of external d and s electrons for Ni (10) and Fe (8), and s and p for Ga (3). The experimentally evaluated chemical composition together with the e/a are summarized in Table 1. There are no significant differences between both sides of the ribbon and the composition agrees with the nominal one. Additionally, point analyses and elemental mappings show a homogeneous distribution of the elements (not shown).

Fig. 2 shows the room temperature XRD patterns taken from both the wheel and the free surfaces of the as-spun ribbon, exhibiting a martensite structure. Small differences in the intensities of peaks between both sides of the ribbon can be observed, due to the highly textured polycrystalline character of the ribbons. The splitting of the {220} reflection of the austenite phase into doublets or triplets is

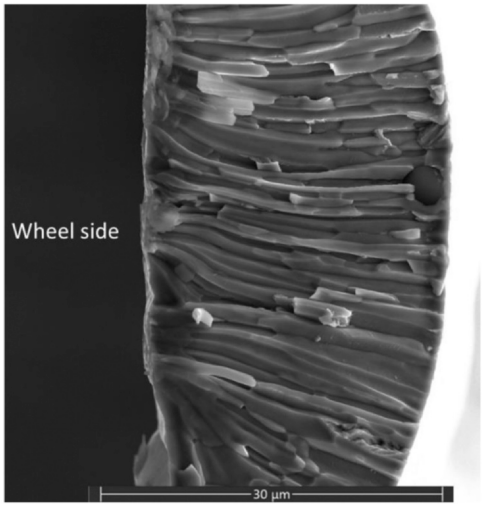

Fig. 1. SEM micrograph in secondary electrons mode of a cross section of the melt-spun ribbon.

Table 1
Average value of chemical composition (at%) and e/a for both sides of melt-spun ribbon and the bulk sample from XRF.

Sample	Ni	Fe	Ga	e/a
Nominal	55	19	26	7.8
Ribbon (free side)	54.72 ± 0.12	19.20 ± 0.16	26.08 ± 0.21	7.79 ± 0.03
Ribbon (wheel side)	54.41 ± 0.11	19.22 ± 0.15	26.37 ± 0.20	7.77 ± 0.03
Bulk	54.64 ± 0.14	19.39 ± 0.11	25.95 ± 0.16	7.79 ± 0.03

usually taken as an evidence for a tetragonally distorted martensite phase, assigned by Wang et al. [24] as space group $I4/mmm$. However, Righi et al. [25] proposed an orthorhombic $Pnnm$ space group with a seven-layered modulation on the basis of a Rietveld analysis of the low-temperature XRD data. On the other hand, Singh et al. [26] and Krenke et al. [27] identified the monoclinic space group $P2/m$ for modulated martensite structures. In order to evaluate the space group and modulated structure of the martensite phase, a Le Bail fitting was performed using the different space groups cited above. All peaks could only be indexed by the monoclinic $P2/m$ space group and the obtained lattice parameters were $a = 4.3138(2)$ Å, $b = 30.2511(17)$ Å, $c = 5.6190(3)$ Å, $\beta = 89.028(5)°$ (GOF = 1.4). It should be noted that $b \sim 7a$ indicates a seven fold increase in the unit cell length along b axis, which is in agreement with transmission electron microscopy observations, showing six extra spots between two fundamental maxima, reported in our previous work [23]. This relation has been related to modulation of the atomic positions in Ni-Mn-Ga systems from both neutron [28] and X-ray diffraction studies [29].

DSC scans at 20 K/min were performed to analyze the MT of the ribbon. The DSC curve registered during a cooling and heating cycle is shown in Fig. 3a along with the record of the previous heating up to 473 K (we considered the cycle this way as we do not expect any irreversible transformation for temperatures below the starting temperature of the cycle). The exothermic and endothermic peaks correspond to the forward and reverse MT, respectively. The onset of the martensitic transformation (martensite start temperature, M_{start}) during cooling and of the reverse martensitic transformations (austenite start temperature, A_{start}) was estimated by the two-tangent method. The calorimetric scans reveal that thermal treatments induce a decrease of the MT temperature as the maximum heating temperature increases, which will be discussed later.

Fig. 3b shows the temperature dependence of magnetization measured at heating/cooling rates of 1 K/min under two different

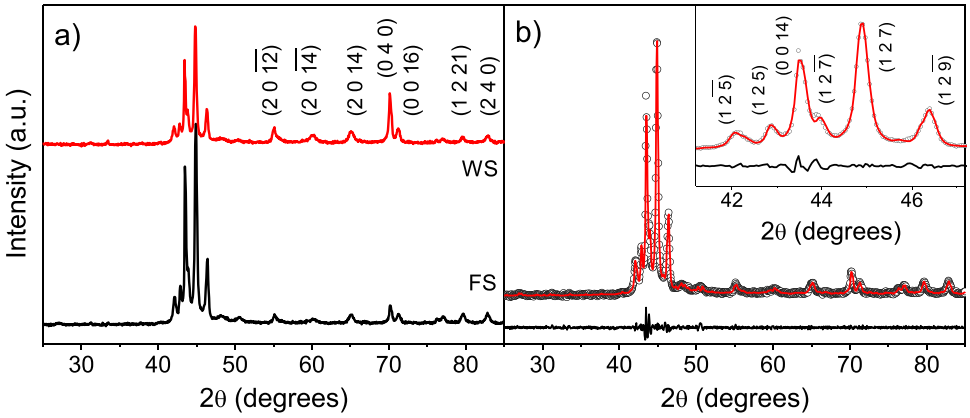

Fig. 2. a) XRD patterns of $Ni_{55}Fe_{19}Ga_{26}$ as-spun ribbon for the wheel, WS, (upper) and the free, FS, (bottom) sides, respectively. b) Le Bail fitting for XRD pattern of the as-spun ribbon (FS) with $P2/m$ space group. The open circles and the solid continuous lines represent observed and calculated patterns, respectively. The difference plot is shown at the bottom. The inset depicts a horizontally zoomed plot in a limited range of 2θ. The Bragg peaks are labeled according to the notation of the monoclinic system usually used to describe the modulated 14M structure.

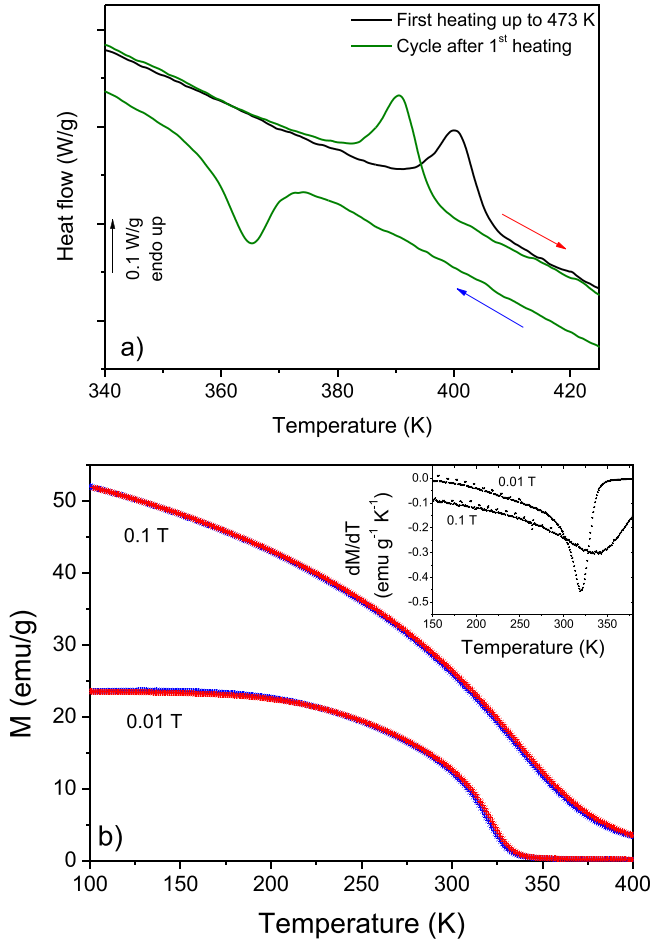

Fig. 3. a) DSC scans of ribbon samples measured at 20 K/min in the vicinity of the martensitic transformation during heating and cooling cycles. Arrows indicate heating and cooling pathways. b) Thermomagnetic measurements on as-prepared ribbon upon cooling (blue) and heating (red) from 400 to 100 K and under different external applied magnetic fields. Inset shows their corresponding dM/dT curves.

magnetic fields. Upon cooling, only a Curie transition has been observed in the $M(T)$ curves. Taking into account the XRD results, this transition should correspond to the magnetic transformation of the 14M modulated structure ($T_C^{14M} = 319$ K). This result supports those obtained by DSC, showing the MT at temperatures close to the limit of measurement range of PPMS.

3.2. Bulk sample

A bulk alloy was obtained by arc-melting. The average chemical composition of the as-prepared sample obtained by XRF is shown in Table 1. Fig. 4 represents XRD patterns of the as-prepared bulk sample (ASB) and after annealing at 1073 K for 24 h and then, immediately, quenched in water (Thermally Treated Bulk sample, TTB). All the peaks in ASB sample can be indexed with a non-modulated tetragonal $L1_0$ structure (space group $I4/mmm$) and the γ phase (space group $Pm\bar{3}m$), confirming the limitation of arc-melting technique to produce single-phase samples. After the thermal treatment, the 14M modulated structure (also found in the as-melted ribbon) is developed. In fact, the Le Bail fit of the pattern reveals the coexistence of two phases, the monoclinic structure corresponding to a martensite phase ($a = 4.32987(16)$ Å, $b = 30.3519(6)$ Å, y $c = 5.5537(4)$ Å) and a cubic structure corresponding to the γ phase ($a = 3.59974(9)$). Again, the relation $b \approx 7a$ indicates that the type of modulation is 14M.

Fig. 5 shows representative SEM images obtained for ASB (left side) and TTB (right side) samples. The images obtained using secondary electrons (Fig. 5a and d) show a typical martensitic morphology, with variants of twinned martensite in the case of the TTB sample. The small black dots are pores created during fabrication process. In the case of the backscattered images, it can be clearly observed that γ crystals are dispersed inside the martensite grains, which contribution was previously detected by XRD. These crystals are more clearly observed in the case of the TTB sample due to the Fe enrichment of the gamma phase with the thermal treatment (see Fig. 5c and f). Table 2 shows the chemical composition obtained by EDS of the phases that exhibit the bulk samples. In spite of the semiquantitative character of this technique, it is evident the Fe enrichment and Ga decrease of the gamma phase in the TTB sample with respect to the ASB one.

The characteristic temperatures of MT were studied by DSC (Fig. 6a and b). It can be observed large exothermic and endothermic peaks upon cooling and heating associated with martensitic and reverse martensitic transformation, respectively. The ASB sample exhibits a broad MT peak around 340 K (on heating). Thermal treatment gets more pronounced MT, which slightly decreased to lower temperatures around 330 K.

The temperature dependences of magnetization of the bulk samples measured at two different magnetic fields are shown in Fig. 6c and d. The thermomagnetic curves reveal a ferromagnetic behavior with a Curie temperature at 285 and 278 K, for ASB and TTB, respectively. Following the XRD results, these Curie transitions

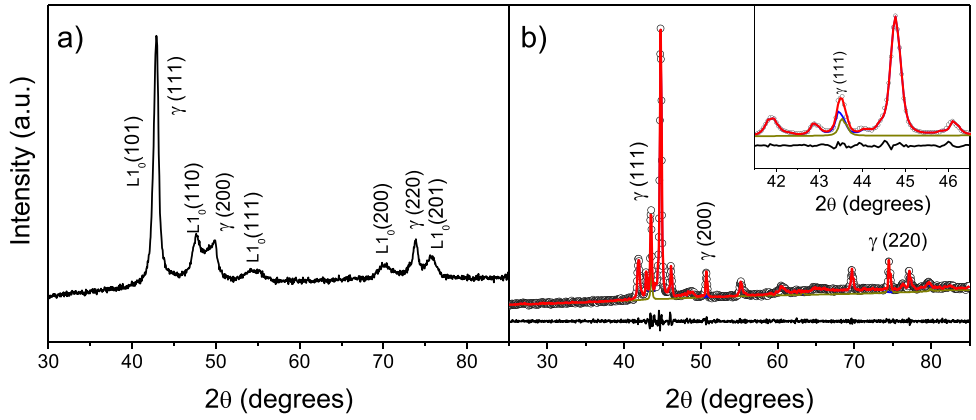

Fig. 4. a) XRD patterns of $Ni_{55}Fe_{19}Ga_{26}$ as-prepared bulk. b) XRD pattern of the TTB sample (open circles) and its Le Bail fitting using $P2/m$ and $Pm\bar{3}m$ space groups (red line). The difference (black line) is shown at the bottom. The inset depicts a horizontally zoomed plot in a limited range of 2θ.

should correspond to the martensite phase. Therefore, upon cooling, transformation sequence is paramagnetic austenite → paramagnetic martensite → ferromagnetic martensite. The MT temperatures are in good agreement with those observed by DSC. The presence of the gamma phase is responsible for a non-zero magnetization above A_{start}.

Table 2
Chemical composition (at%) and e/a for the bulk samples obtained by EDS.

	Martensite phase				Gamma phase		
Sample	Ni	Fe	Ga	e/a	Ni	Fe	Ga
ASB	55(2)	19(2)	26(3)	7.80	56(2)	24(2)	20(3)
TTB	56(2)	18(2)	26(3)	7.82	56(2)	28(2)	16(3)

4. Discussion

The influence of the production method on magneto-structural behavior has been systematically investigated. In order to evaluate the stability of MT in the studied samples, different thermal cycles were done up to a higher maximum temperature each time. Fig. 7 shows, as a function of the upper limit temperature reached in each cycle, the evolution of the parameters of the MT (M_{start} and A_{start}, and the average transformation heat in the forward and reverse transformation). For the ribbon sample it can be observed that the temperature at which the MT occurs continuously decreases with

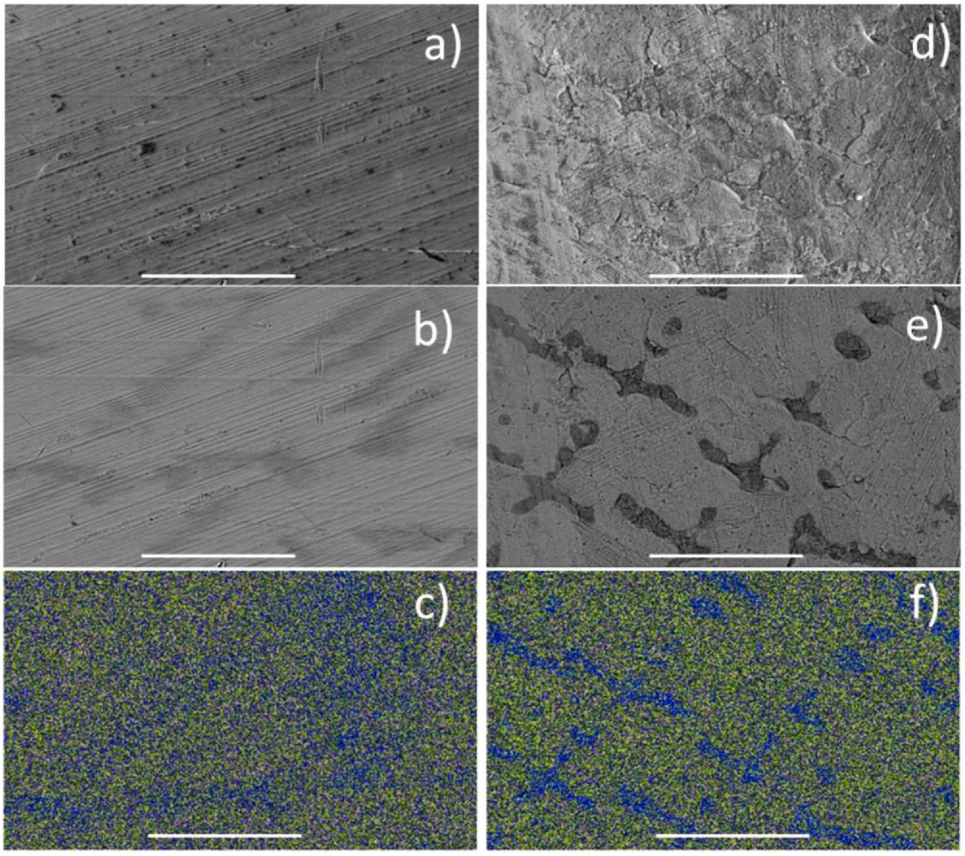

Fig. 5. SEM micrographs obtained using secondary (a and d) and backscattered electrons (b and e) and corresponding compositional maps obtained by EDS (c and f). a–c correspond to ASB sample and d–f to TTB sample. The horizontal bar corresponds to 50 µm. Ni, Fe and Ga elements are represented in green, blue and magenta, respectively.

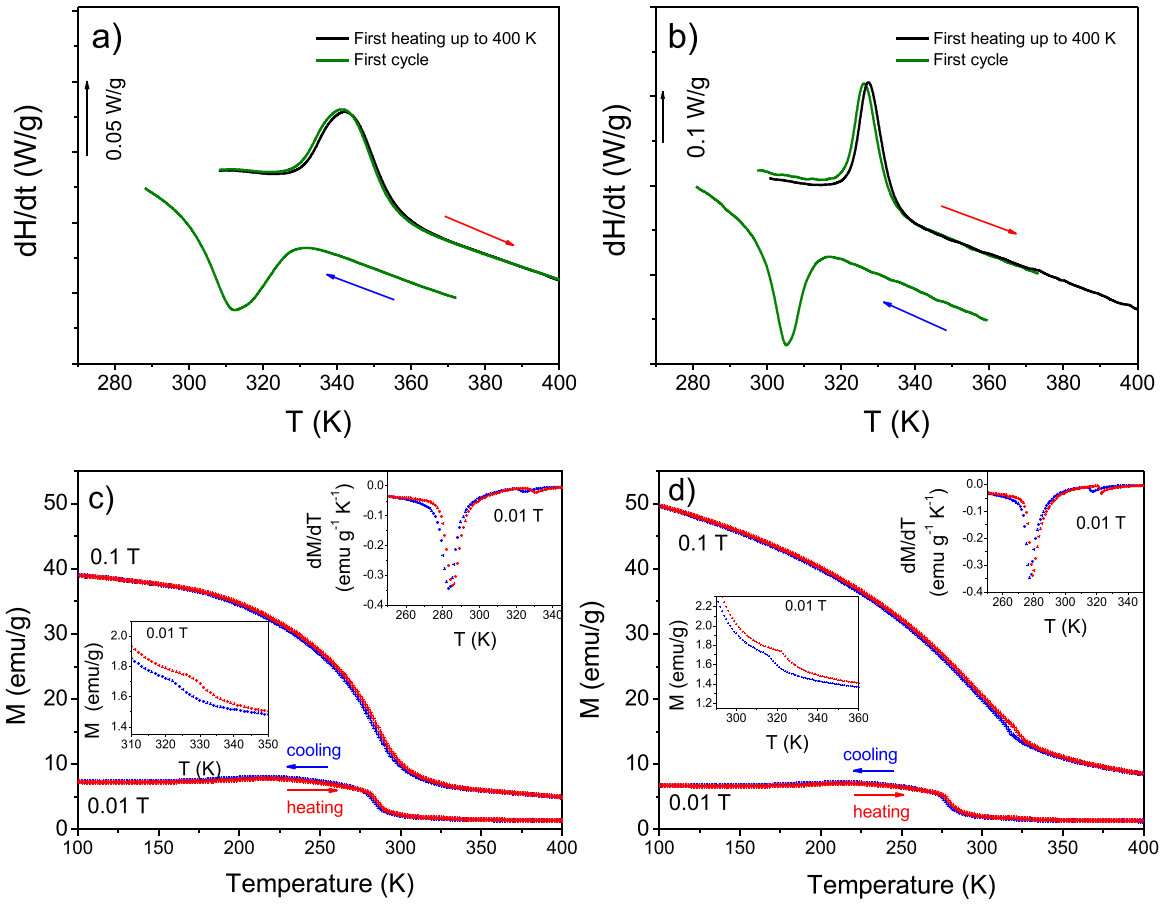

Fig. 6. a) DSC curves measured at 20 K/min in the vicinity of the MT during continuous heating and cooling cycles for a) as-prepared, ASB, and b) thermally treated, TTB, bulk samples. Arrows indicate heating and cooling pathways. Thermomagnetic measurements upon cooling and heating from 400 to 100 K under different external magnetic fields for c) ASB and d) TTB samples. Upper insets in c) and d) show the corresponding dM/dT curves at 0.01 T. Middle insets in c) and d) depict a zoomed plot in a limited range of temperatures.

increasing the upper limit temperature. The thermal hysteresis, defined as A_{start}-M_{start}, is practically constant until the enthalpy of transformation drops significantly (for temperatures higher than 773 K), which could be associated to the precipitation of the gamma phase. These results are in agreement with those collected by Tolea et al. [30], where it is shown that the heat treatments above MT promote a shift to lower temperatures in ribbons of Ni-Fe-Ga-Co composition. In any case, the results obtained suggest that the ribbon undergoes a structural modification during the heat treatments performed. In the case of treatments at low temperatures (< 573 K), relaxation of stresses stored during fabrication of the ribbons occurs. Treatments at high temperatures (> 773 K) induce precipitation and growth of the gamma phase [23].

Unlike the results obtained for the ribbon, the parameters associated to MT remain practically constant in the case of the bulk samples, at least for the range of temperatures analyzed. As it was previously shown (see Fig. 6a and b), MT occurs at slightly higher temperatures for the ASB sample than for the TTB one. This displacement could be associated with the Fe enrichment of the gamma phase in the case of the TTB sample. Moreover, both transformation enthalpy and temperature at which the transition occurs are lower for the bulk sample than for the ribbon sample, due to the existence of the gamma phase. This phase, on the one hand, limits the fraction of transformable phase, reducing the transformation enthalpy and, on the other hand, modifies the electronic valence concentration per atom of the martensite phase, with which MT exhibits a strong dependence [31]. Therefore, enthalpy change could be used to estimate the fraction of the gamma phase in the TTB sample if a 100% of the 14M structure is assumed for the as-spun ribbon. The results of this analysis lead to an approximately 20% of the gamma phase in the TTB and ASB samples. Assuming the composition for the alloy shown in Table 1 ($Ni_{54.64}Fe_{19.39}Ga_{25.95}$) and the composition of the gamma phase shown in Table 2 ($Ni_{56}Fe_{24}Ga_{20}$ for ASB and $Ni_{56}Fe_{28}Ga_{16}$ for TTB), we can roughly estimate the composition of both phases and from them the e/a values, resulting 7.72 and 7.67 for the ASB and TTB samples, respectively. The errors of this estimation as well as the e/a values presented in Table 2 are above 10%, and thus the quantitative values must be taken with caution. However, qualitatively, the enrichment in Fe and impoverishment in Ga of the gamma phase must indirectly imply a decrease in the e/a value of the martensite phase, which is pointed by the EDS results in Table 2.

In order to show the structural modification of the ribbon and to analyze the decrease of the enthalpy in the successive thermal cycles, different pieces of ribbon were heated at 10 K/min up to different temperatures and then annealed for 10 min. It should be mentioned that the annealing temperatures, although above the martensitic transition temperature of the as-spun ribbon, are below the order-disorder phase transition $L2_1$-B2 temperature (~ 973 K) [32].

Fig. 8 shows XRD patterns of the annealed ribbons along with that of the as-spun ribbon. As it was previously indicated, the structure of the as-spun ribbon corresponds to a 14M modulated phase. The annealings at 673 and 773 K only produce a small variation of the lattice parameters, which modifies the b/a ratio. In fact,

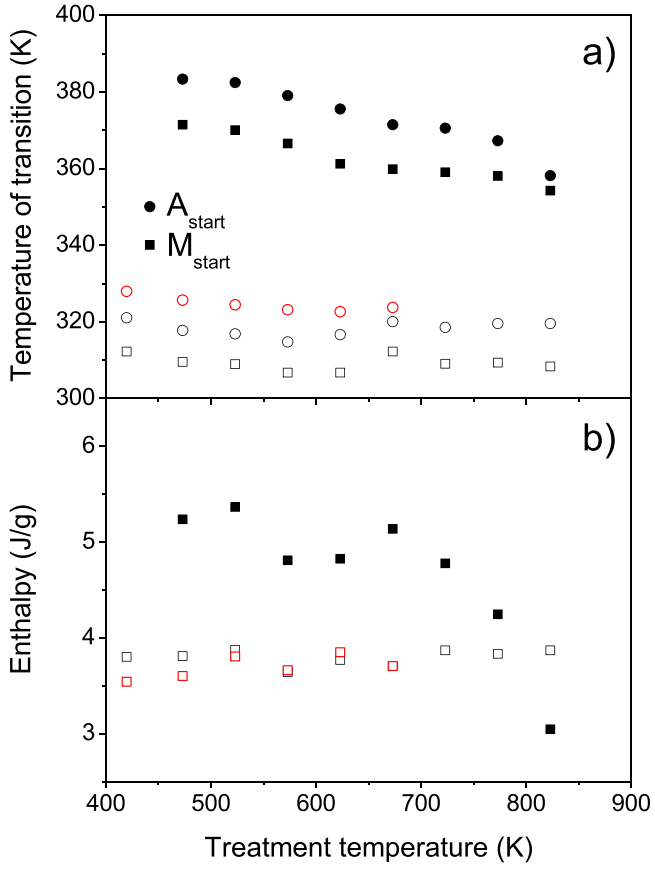

Fig. 7. a) Temperatures corresponding to the martensitic transformation start, M_{start}, during cooling and reverse martensitic start temperature, A_{start}, and b) average heat of transformation as a function of the upper limit temperature attained in each cycle. Filled symbols are used for ribbon samples and empty symbols are used for as-prepared (red) and thermally treated (black) bulk samples.

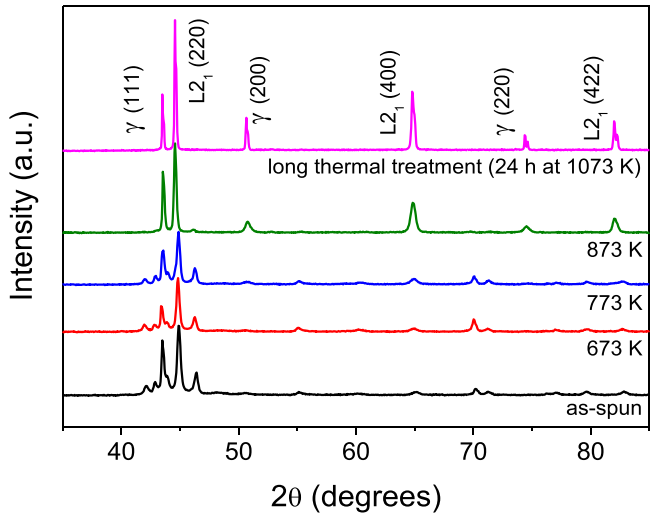

Fig. 8. XRD patterns of $Ni_{55}Fe_{19}Ga_{26}$ ribbons annealed 10 min at the marked temperatures along with the pattern of the ribbon submitted to the same long thermal treatment of the bulk sample.

when the same type of Le Bail fitting (not shown) is applied to these patterns, $b/a = 6.68$ and 6.67 for the samples annealed at 673 and 773 K, respectively, being 7.01 for the as-spun ribbon.

The variation of the lattice parameters is related to the precipitation of the γ phase, which modifies the composition of the modulated structure and limits the proportion of main phase that

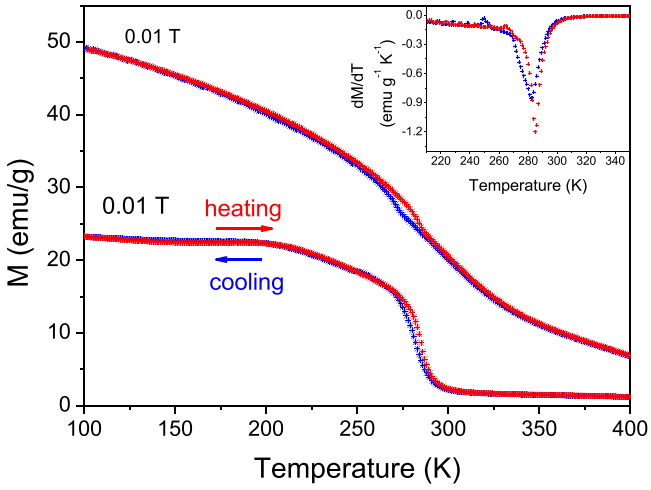

Fig. 9. Thermomagnetic measurements upon cooling and heating between 400 and 100 K on thermally treated ribbon sample at 1073 K for 24 h under different external magnetic fields. Inset shows the corresponding dM/dT curves at 0.01 T.

can transform and, therefore, decreases the transition enthalpy obtained by DSC. After annealing at 873 K, the monophasic character of the ribbon clearly disappears, and the martensitic modulated structure gives rise to two phases, the austenite and γ phases, although small traces of the modulated phase can still be observed (see maximum at ~ $2\theta = 46^{\circ}$). Therefore, the MT shift towards lower temperatures can be understood as a progressive destabilization of the 14M modulated phase due to the precipitation of the gamma phase, leading to a stabilization of the austenite phase at room temperature (RT).

In order to completely stabilize the austenite phase at RT, pieces of ribbon were annealed at 1073 K for 24 h in a quartz ampoule filled with Ar and then immediately quenched in water sample (same treatment performed to the bulk sample), that will be called TTR (Thermally Treated Ribbon). The corresponding XRD pattern of this sample (Fig. 8) exhibits a mixture of two phases that can be indexed as $L2_1$ austenite and γ phases. Fig. 9 shows the temperature dependence of magnetization of sample. Upon cooling, the transformation sequence is paramagnetic austenite → ferromagnetic austenite → ferromagnetic martensite. It means that the ferromagnetic-paramagnetic transformation is finished (or nearly finished) before the martensite starts to form (see inset Fig. 9). Therefore, the observed Curie temperature corresponds to the austenite phase, $T_C^A = 285$ K, which is lower than T_C^{14M}. On the other hand, $A_{start} = 265$ K and $M_{start} = 250$ K.

Table 3 shows the MT temperatures, T_M, and the Curie temperatures of the martensite, T_C^M, and the austenite, T_C^A, phases for the different studied samples obtained by magnetometry measurements. MT behavior is significantly different between them. While T_M is practically constant in the case of the bulk, this parameter changes by ~ 150 K in the ribbons. This significant variation can be related to the grain refinement, internal stresses and high density of

Table 3
Characteristic transformation temperatures (martensitic transformation T_M and Curie temperatures of the martensite, T_C^M, and the austenite T_C^A, phases), for the as-prepared and thermal treated samples (TTR and TTB), obtained by magnetothermal measurements. In the case of the T_C^M the structure of the martensite phase has been indicated. ND: Not-detected.

Sample		T_M (K)	T_C^M (K)	T_C^A (K)
Ribbon	As-prepared	400	320 (14M)	ND
	TTR	257	ND	285
Bulk	As-prepared	328	283 ($L1_0$)	ND
	TTB	320	278 (14M)	ND

lattice defects such as dislocations and vacancies introduced during the melt-spinning process [33], leading to a high dependence of T_M with the thermal treatments. On the other hand, although it has been reported that T_M depends on several factors, the dominant one is the chemical composition [14,34]. Thus, e/a effect should be taken into account in the studied samples due to the precipitation of the γ phase developed after the thermal treatments.

Although the Curie temperatures of the 14M modulated phase of the ribbon and the bulk samples differ from each other, this difference is smaller, as expected, than the differences found for T_M. In fact, the dependence of Curie temperatures, T_C^M and T_C^A, on e/a is less pronounced than in the case of T_M [35]. It is also worth mentioning the small variation of T_M (few degrees) after the bulk is thermally treated even despite the modification of the structure of the martensite. Finally, the T_C^A was only detected in the case of the quenched ribbon, the bulk samples being paramagnetic in the temperature range in which austenite is detected.

5. Conclusions

Nickel-rich polycrystalline $Ni_{55}Fe_{19}Ga_{26}$ Heusler alloy was produced using melt-spinning and conventional casting techniques. The microstructure and magnetostructural transformation behavior have been analyzed. The main conclusions obtained are:

- The crystal structure of sample prepared in a ribbon shape exhibits a single-phase martensite modulated 14M structure at room temperature. The arc-melting technique did not allow us to obtain a single-phase sample, obtaining a coexistence of a non-modulated martensite structure and gamma phase at room temperature. However, the modulated phase in the bulk is developed after a long-term heat treatment followed by water quenching. This treatment also promotes an Fe enrichment of the gamma phase.
- Characteristic temperatures of the martensitic transformation are lower for the bulk sample with respect to the melt-spun ribbons. This may be connected with the change of the e/a parameter due to the precipitation of the gamma phase in the case of the bulk.
- For the bulk alloy the parameters of the transformation (martensite temperature and enthalpy) are practically constant in the range of temperatures analyzed here, whereas these parameters significantly change in the case of the ribbons; both decrease with the increase of the annealing temperature.
- The martensitic transformation takes place in the paramagnetic regime in the case of the as-spun ribbon and the thermally treated bulk.

CRediT authorship contribution statement

A.F. Manchón-Gordón: Conceptualization, Experiments, Formal analysis, Writing – original draft. **J.J. Ipus:** Experiment, Supervision, Writing – review & editing. **M. Kowalczyk**: Experiment, Supervision, Writing – review & editing. **A. Wójcik:** Experiment, Supervision, Writing – review & editing. **J.S. Blázquez:** Conceptualization, Methodology, Supervision, Writing – original draft, Resources. **C.F. Conde**: Methodology, Supervision, Writing – review & editing. **W. Maziarz:** Resources, Writing – review & editing. **P. Švec Sr.:** Samples, Resources, Supervision, Writing – review & editing. **T. Kulik:** Resources, Writing – review & editing. **A. Conde**: Resources, Methodology, Supervision, Writing – review & editing.

Declaration of Competing Interest

The authors declare that they have no known competing financial interests or personal relationships that could have appeared to influence the work reported in this paper.

Acknowledgements

This work was supported by AEI/FEDER-UE (Projects US-1260179 and P18-RT-746) and the PAI of the Regional Government of Andalucía. Support of projects VEGA [Grant no. 2/0144/21] and APVV [Grant no. APVV-19-0369] is acknowledged. A.F. Manchón-Gordón acknowledges a VPPI-US Fellowship. The magnetic measurements were performed in the frame of the polish National Centre for Research and Development funding (Grant no.: Techmatstrateg2/410941/4/NCBR/2019).

References

[1] K. Ullakko, J.K. Huang, C. Kantner, R.C. Ohandley, V.V. Kokorin, Large magnetic-field-induced strains in Ni_2MnGa single crystals, Appl. Phys. Lett. 69 (1996) 1966–1968, https://doi.org/10.1063/1.117637
[2] A. Sozinov, A.A. Likhachev, N. Lanska, K. Ullakko, Giant magnetic-field-induced strain in NiMnGa seven-layered martensitic phase, Appl. Phys. Lett. 80 (2002) 1746–1748, https://doi.org/10.1063/1.1458075
[3] C.B. Jiang, Y. Muhammad, L.F. Deng, W. Wu, H.B. Xu, Composition dependence on the martensitic structures of the Mn-rich NiMnGa alloys, Acta Mater. 52 (2004) 2779–2785, https://doi.org/10.1016/j.actamat.2004.02.024
[4] H.E. Karaca, I. Karaman, B. Basaran, Y.J. Chumlyakov, H.J. Maier, Magnetic field and stress induced martensite reorientation in NiMnGa ferromagnetic shape memory alloy single crystals, Acta Mater. 54 (2006) 233–245, https://doi.org/10.1016/j.actamat.2005.09.004
[5] M. Chmielus, I. Glavatskyy, J.-U. Hoffmann, V.A. Chernenko, R. Schneider, P. Muellner, Influence of constraints and twinning stress on magnetic field-induced strain of magnetic shape-memory alloys, Scr. Mater. 64 (2011) 888–891, https://doi.org/10.1016/j.scriptamat.2011.01.025
[6] J. Pons, E. Cesari, C. Segui, F. Masdeu, R. Santamarta, Ferromagnetic shape memory alloys: alternatives to Ni-Mn-Ga, Mater. Sci. Eng. A-Struct. Mater. Prop. Microstruct. Process. 481 (2008) 57–65, https://doi.org/10.1016/j.msea.2007.02.152
[7] M. Imran, X.X. Zhang, Ferromagnetic shape memory Ni-Fe-Ga alloy foams for elastocaloric cooling, J. Phys. D: Appl. Phys. 53 (2020) 245503, https://doi.org/10.1088/1361-6463/ab7df1 245503.
[8] M. Imran, X.X. Zhang, M.F. Qian, L. Geng, Enhancing the elastocaloric cooling stability of Ni-Fe-Ga alloys via introducing pores, Adv. Eng. Mater. 22 (2020) 1901140, https://doi.org/10.1002/adem.201901140
[9] V.I. Nikolaev, S.I. Stepanov, P.N. Yakushev, V.M. Krymov, S.B. Kustov, Burst-like shape recovery and caloric effects in Ni-Fe-Ga-Co single crystalline shape memory alloys, Intermetallics 119 (2020) 106709, https://doi.org/10.1016/j.intermet.2020.106709
[10] R. Santamarta, J. Font, J. Muntasell, F. Masdeu, J. Pons, E. Cesari, J. Dutkiewicz, Effect of ageing on the martensitic transformation of Ni-Fe-Ga alloys, Scr. Mater. 54 (2006) 1105–1109, https://doi.org/10.1016/j.scriptamat.2005.11.062
[11] J. Font, J. Muntasell, R. Santamarta, J. Pons, E. Cesari, V. Recarte, J.I. Perez-Landazabal, C. Gomez-Polo, J. Dutkiewicz, Thermal stability and ordering effects in Ni-Fe-Ga ferromagnetic shape memory alloys, Mater. Sci. Eng. A-Struct. Mater. Prop. Microstruct. Process. 481 (2008) 262–265, https://doi.org/10.1016/j.msea.2007.01.183
[12] H.J. Yu, H. Fu, Z.M. Zeng, J.X. Sun, Z.G. Wang, W.L. Zhou, X.T. Zu, Phase transformations and magnetocaloric effect in NiFeGa ferromagnetic shape memory alloy, J. Alloy. Compd. 477 (2009) 732–735, https://doi.org/10.1016/j.jallcom.2008.10.143
[13] J.M. Barandiaran, V.A. Chernenko, P. Lazpita, J. Gutierrez, J. Feuchtwanger, Effect of martensitic transformation and magnetic field on transport properties of Ni-Mn-Ga and Ni-Fe-Ga Heusler alloys, Phys. Rev. B 80 (2009) 104404, https://doi.org/10.1103/PhysRevB.80.104404
[14] D. Pal, K. Mandal, Magnetocaloric effect and magnetoresistance of Ni-Fe-Ga alloys, J. Phys. D: Appl. Phys. 43 (2010) 455002, https://doi.org/10.1088/0022-3727/43/45/455002
[15] Z.H. Liu, M. Zhang, Y.T. Cui, Y.Q. Zhou, W.H. Wang, G.H. Wu, X.X. Zhang, G. Xiao, Martensitic transformation and shape memory effect in ferromagnetic Heusler alloy Ni_2FeGa, Appl. Phys. Lett. 82 (2003) 424–426, https://doi.org/10.1063/1.1534612
[16] N.V. Rama Rao, R. Gopalan, M. Manivel Raja, V. Chandrasekaran, K.G. Suresh, Mössbauer studies on structural ordering and magnetic properties of melt-spun Ni–Fe–Ga ribbons, Applied Physics Letters 93 (2008) 202503, https://doi.org/10.1063/1.3028342
[17] Y. Zhang, Q. Zheng, W. Xia, J. Zhang, J. Du, A. Yan, Enhanced large magnetic entropy change and adiabatic temperature change of $Ni_{43}Mn_{46}Sn_{11}$ alloys by a rapid solidification method, Scr. Mater. 104 (2015) 41–44, https://doi.org/10.1016/j.scriptamat.2015.04.004
[18] A. Wojcik, W. Maziarz, M. Szczerba, M. Kowalczyk, E. Cesari, J. Dutkiewicz, Structure and inverse magnetocaloric effect in Ni-Co-Mn-Sn(Si) Heusler alloys, Intermetallics 100 (2018) 88–94, https://doi.org/10.1016/j.intermet.2018.06.004
[19] J. Liu, N. Scheerbaum, O. Gutfleisch, Comparative study of structural and magnetic properties of bulk and powder $Ni_{52}Fe_{17}Ga_{27}Co_4$ magnetic shape memory alloy, IEEE Trans. Magn. 44 (2008) 3025–3027, https://doi.org/10.1109/TMAG.2008.200

[20] H. Okumura, K. Uemura, Influence of quenching rate on the magnetic and martensitic properties of Ni-Fe-Ga melt-spun ribbons, J. Appl. Phys. 108 (2010) 043910, https://doi.org/10.1063/1.3465613
[21] I. Unzueta, D.A. de R-Lorente, E. Cesari, V. Sanchez-Alarcos, V. Recarte, J.I. Perez-Landazabal, J.A. Garcia, F. Plazaola, Experimental observation of vacancy-assisted martensitic transformation shift in Ni-Fe-Ga alloys, Phys. Rev. Lett. 122 (2019) 165701, https://doi.org/10.1103/PhysRevLett.122.165701
[22] A.F. Manchon-Gordon, R. Lopez-Martin, J.J. Ipus, J.S. Blazquez, P. Svec, C.F. Conde, A. Conde, Kinetic analysis of the transformation from 14M martensite to L21 austenite in Ni-Fe-Ga melt spun ribbons, Metals 11 (2021) 849, https://doi.org/10.3390/met11060849
[23] A.F. Manchon-Gordon, J.J. Ipus, M. Kowalczyk, A. Wojcik, J.S. Blazquez, C.F. Conde, W. Maziarz, P. Svec, T. Kulik, A. Conde, Effect of pressure on the phase stability and magnetostructural transitions in nickel-rich NiFeGa ribbons, Journal of Alloys and Compounds 844 (2020) 156092, https://doi.org/10.1016/j.jallcom.2020.156092
[24] W.H. Wang, Z.H. Liu, J. Zhang, J.L. Chen, G.H. Wu, W.S. Zhan, T.S. Chin, G.H. Wen, X.X. Zhang, Thermoelastic intermartensitic transformation and its internal stress dependency in $Ni_{52}Mn_{24}Ga_{24}$ single crystals, Phys. Rev. B 66 (2002) 052411, https://doi.org/10.1103/PhysRevB.66.052411
[25] L. Righi, F. Albertini, G. Calestani, L. Pareti, A. Paoluzi, C. Ritter, P.A. Algarabel, L. Morellon, M.R. Ibarra, Incommensurate modulated structure of the ferromagnetic shape-memory Ni_2MnGa martensite, J. Solid State Chem. 179 (2006) 3525–3533, https://doi.org/10.1016/j.jssc.2006.07.005
[26] S. Singh, R. Rawat, S.R. Barman, Existence of modulated structure and negative magnetoresistance in Ga excess Ni-Mn-Ga, Appl. Phys. Lett. 99 (2011) 021902, https://doi.org/10.1063/1.3604015
[27] T. Krenke, M. Acet, E.F. Wassermann, X. Moya, L. Manosa, A. Planes, Martensitic transitions and the nature of ferromagnetism in the austenitic and martensitic states of Ni–Mn–Sn alloys, Phys. Rev. B 72 (2005) 014412, https://doi.org/10.1103/PhysRevB.72.014412
[28] P.J. Brown, J. Crangle, T. Kanomata, M. Matsmuoto, K.U. Neumann, B. Ouladdiaf, K.R.A. Ziebeck, The crystal structure and phase transitions of the magnetic shape memory compound Ni_2MnGa, J. Phys.-Condens. Matter 14 (2002) 10159–10171, https://doi.org/10.1088/0953-8984/14/43/313
[29] S. Singh, M. Maniraj, S.W. D'Souza, R. Ranjan, S.R. Barman, Structural transformations in Mn_2NiGa due to residual stress, Appl. Phys. Lett. 96 (2010) 081904, https://doi.org/10.1063/1.3318461
[30] F. Tolea, M. Sofronie, A.D. Crisan, M. Enculescu, V. Kuncser, M. Valeanu, Effect of thermal treatments on the structural and magnetic transitions in melt-spun Ni-Fe-Ga-(Co) ribbons, J. Alloy. Compd. 650 (2015) 664–670, https://doi.org/10.1016/j.jallcom.2015.07.296
[31] X. Moya, L. Manosa, A. Planes, T. Krenke, M. Acet, E.F. Wassermann, Martensitic transition and magnetic properties in Ni-Mn-X alloys, Mater. Sci. Eng. A-Struct. Mater. Prop. Microstruct. Process. 438 (2006) 911–915, https://doi.org/10.1016/j.msea.2006.02.053
[32] K. Oikawa, T. Ota, T. Ohmori, Y. Tanaka, H. Morito, A. Fujita, R. Kainuma, K. Fukamichi, K. Ishida, Magnetic and martensitic phase transitions in ferromagnetic Ni-Ga-Fe shape memory alloys, Appl. Phys. Lett. 81 (2002) 5201–5203, https://doi.org/10.1063/1.1532105
[33] V. Sanchez-Alarcos, V. Recarte, J.I. Perez-Landazabal, G.J. Cuello, Correlation between atomic order and the characteristics of the structural and magnetic transformations in Ni-Mn-Ga shape memory alloys, Acta Mater. 55 (2007) 3883–3889, https://doi.org/10.1016/j.actamat.2007.03.001
[34] V.A. Chernenko, Compositional instability of beta-phase in Ni-Mn-Ga alloys, Scr. Mater. 40 (1999) 523–527, https://doi.org/10.1016/S1359-6462(98)00494-1
[35] T. Gottschall, K.P. Skokov, D. Benke, M.E. Gruner, O. Gutfleisch, Contradictory role of the magnetic contribution in inverse magnetocaloric Heusler materials, Phys. Rev. B 93 (2016) 184431, https://doi.org/10.1103/PhysRevB.93.184431